Hindawi
Advances in Materials Science and Engineering
Volume 2023, Article ID 6522013, 11 pages
https://doi.org/10.1155/2023/6522013

Research Article

Experimental and Numerical Analysis of the Thermal Conductivity of SiC_f/SiC Composites

Zhaoguo Mi,[1] **Zhenhua Chen**,[2] **and Weihua Yang**[1]

[1]*Nanjing University of Aeronautics and Astronautics, Nanjing, China*
[2]*China Aviation Development, Hunan Power Machinery Research Institute, Zhuzhou, China*

Correspondence should be addressed to Weihua Yang; yangwh@nuaa.edu.cn

Received 5 September 2022; Revised 23 February 2023; Accepted 1 March 2023; Published 29 April 2023

Academic Editor: Yasir Nawab

SiC fiber-reinforced silicon matrix (SiC_f/SiC) composites are of significant interest for the aircraft engine. The thermal conductive behaviors of [0-90-0]s SiC_f/SiC composites along in-plane and out-of-plane (thickness) directions were reported in this paper. The thermal conductivity of the SiC_f/SiC composite was tested by using the steady-state measuring apparatus. Then, the thermal conductivity of the SiC matrix was predicted by finite element analysis (FEA). The representative volume element (RVE) models of SiC_f/SiC composites were built, and FEA was used to investigate thermal conductive behaviors. It was found that the thermal conductivity along the fiber radial direction was greater than it was in the axial direction in the SiC_f/SiC composite and that the thermal conductivity of the out-of-plane direction is lower than that of the in-plane one. The thermal conductivity of the SiC_f/SiC composite in the in-plane direction at room temperature was 31.1 $Wm^{-1}K^{-1}$ and 28.5 $Wm^{-1}K^{-1}$, and the thermal conductivity in the thickness direction was 24.9 $Wm^{-1}K^{-1}$. The experimental thermal conductivity showed a good agreement with the thermal conductivity of FEA.

1. Introduction

SiC fiber-reinforced SiC matrix (SiC_f/SiC) composites have been widely used in many fields including aerospace and aircraft, nuclear energy, and other fields due to their excellent properties, such as their high specific strength and stiffness, high-temperature resistance, high mechanical strength at high temperatures, and outstanding corrosion resistance [1]. SiC/SiC composites are used in high thermostructural applications with long-time exposures compared with other ceramic matrix composites (CMCs) [2]. These composites are often used as ideal hot-end components, and their temperature distribution under high-temperature conditions needs to be predicted during design. Therefore, the accurate evaluation of the thermal conductivity of the SiC_f/SiC composite is of great significance in understanding and designing SiC_f/SiC composites.

The thermal conductivity of SiC_f/SiC composites is anisotropic, due to their fiber architecture. There are many methods for measuring the thermal conductivity of anisotropic materials, such as the steady-state thermal reflectivity method [3], the transient plane source method [4, 5], the hot wire method [6], the steady-state protection hot plate method [7], and other steady-state methods [8, 9]. Zhang et al. [10] used three methods to measure the anisotropic thermal conductivity of CMCs. The thermal conductivity of the 200 mm × 200 mm × 15 mm sample in thickness was measured by the steady-state method, then, the sample was cut into very thin strips, and the in-plane thermal conductivity was measured after recombination. The thermal conductivity of the 50 mm × 50 mm × 15 mm samples was measured by the transient plane source (TPS) method. The hot wire method was used to measure the equivalent thermal conductivity in the plane perpendicular to the hot wire, and the thermal conductivity in the in-plane direction and the thickness direction was calculated by the formula. By comparison, the maximum deviation of the steady-state measurement method compared with the transient measurement of thermal conductivity was 18.1%. With the development of numerical research, the

representative volume element (RVE) model was proposed for the CMC composite, and thermal conductivity was studied by numerical methods based on the RVE model. Through the comparison of experimental and numerical results, it was verified that the RVE model numerically predicts the thermal conductivity of CMC feasibility. Penide-Fernandez and Sansoz [11] measured 40 samples with a thickness of 0.55 mm and an area of 40 mm^2 by the TPS method, obtained the thermal conductivity with a two-dimensional braided ceramic fiber, and then compared the thermal conductivity obtained by the FEA with the experimental results. It is proposed that the accuracy of material geometry can effectively obtain the anisotropic thermal conductivity by FEA. Kai Dong et al. [12] used the steady-state method to measure the in-plane thermal conductivity of CMCs and the TPS method to measure the thermal conductivity in the thickness direction. Then, they used the FEA to compare the FEA results and the experimental measurement results. The experimental result showed a good agreement with those of FEA.

It is a normal method that established an RVE model for predicting CMCs thermal conductivity by FEA [13–16]. The FEA method needs the thermal conductivity of the fibers, interface layer, and matrix. The fact is that the thermal conductivity of a matrix changes and is hard to measure. The manufacturing process of CMCs includes hot pressing (HP), spark plasma sintering (SPS), and nonsintering techniques including chemical vapor infiltration (CVI), reactive melt infiltration (RMI), and precursor infiltration and pyrolysis (PIP) [17]. The properties of CMCs are related to the manufacturing process, and there are certain differences in the thermal conductivity of SiC_f/SiC composites prepared by different processes. SiC/SiC composites have different levels of pores and other impurities in the SiC matrix due to different manufacturing processes. Cho and Kim [18] studied the effects of different grain sizes, lattice oxygen content, and α-SiC content on the thermal conductivity of SiC ceramics, and it can be seen from the comparison of measurement results that the thermal conductivity of SiC ceramics is between 55 W/(mK) and 225 W/(mK). Li et al. [19] studied the property changes of SiC ceramic materials by combining stereolithography with reactive melt permeation technology. The results show that the higher the concentration of phenolic resin solution during the manufacturing process, the higher the thermal conductivity of the sintered SiC ceramic. Wang et al. [20] established an RVE model for a SiC_f/SiC composite. Then, they studied the effect of porosity on the calculation of effective thermal conductivity of continuous SiC fiber-reinforced SiC matrix composites by the finite element method. Therefore, the thermal conductivity of the SiC matrix must be obtained before using the FEA method to predict the thermal conductivity of any SiC/SiC composites. However, present studies have rarely considered differences in the thermal conductivity of the SiC matrix for using the FEA method.

The proportions of components in the manufacturing process of SiC_f/SiC composites, fiber-weaving methods, and manufacturing processes will affect the thermal conductivity of CMCs. Presently, some research reported the thermal conductivity of some SiC_f/SiC composites, but it is not enough to know the law of thermal conductivity of SiC_f/SiC composites. Pek et al. [21] used the time-domain thermal response rate (TDTR) method to measure the thermal conductivity distribution of SiC_f/SiC composites and obtained the thermal conductivity at 1000°C as 29 $Wm^{-1}K^{-1}$ by taking the weighted average. Hye-gyu and Wooseok [22] established an RVE model for 3D braided SiC_f/SiC composites and predicted thermal conductivity using the finite element method.

In this study, the thermal conductivity of laminated [0-90-0]s SiC_f/SiC composites in-plane and out-of-plane directions was measured by the steady-state method. An improved FEA thermal conductivity prediction method was proposed. The improved FEA method needs to measure the thermal conductivity in one direction. First, the thermal conductivity of the SiC matrix was predicted, and then, the anisotropic thermal conductivity of SiC_f/SiC composites was predicted. Comparing the experimental results with the numerical simulation results, the feasibility of the method combining experiment and numerical simulations was verified for predicting the thermal conductivity of the SiC_f/SiC composite. There are two methods to research the thermal conductivity of composites, experiment and FEA methods. Generally, experiment methods need to fabricate the special sample, but the sample is hard to make. The FEA method needs the geometry model and the thermal conductivity of the fibers, interface layer, and matrix. The thermal conductivity of the SiC matrix is uncertain, due to the impurity like Si and others and voids. Combining these two methods in this paper can simplify the experiment and predict the thermal conductivity of CMCs more accurately. In addition, the anisotropic thermal conductivity of a SiC_f/SiC composite fabricated by the melt infiltration (MI) method was reported.

2. Material and Experimental Procedure

2.1. Composite Material. In this study, the samples of a square plate with a thickness of 3.5 mm and a length of 110 mm were fabricated by the melt infiltration (MI) method. The volume fraction of the SiC fibers added in the SiC matrix is 24%, and the average diameter of fibers is 10.9 μm. By counting the SEM results, the average interface layer thickness is 0.3 μm. The interface layer, which connects the fiber and matrix, plays an important role in determining the properties of the composites. Pyrolytic carbon (PyC) and hexagonal boron nitride (h-BN) are considered the effective interface layers for SiC_f/SiC composites thanks to their layered microstructure. However, the PyC interface layer is easily oxidized in the oxidizing atmosphere even at lower temperatures, resulting in the degradation of the mechanical properties of SiC_f/SiC composites. The BN interface layer will effectively improve the oxidation resistance of SiC_f/SiC composites [23]. A thin boron nitride (BN) interphase produced was deposited first on the surfaces of SiC fibers by the chemical vapor infiltration (CVI) process. The coated SiC fibers were then wetted with phenolic resin to transform into SiC prepregs. The prepregs obtained green bodies via

thermal curing of the phenolic resin. The green bodies were subsequently pyrolyzed to convert the phenolic resin into a carbon source, which was used for the following silicon infiltration process to form a SiC matrix by reaction of carbon with silicon.

The fiber architecture was cross-ply [0°-90°-0°]s. Figure 1 shows an SEM image of the local section of the SiC_f/SiC composites. The direction of the white arrow is the out-of-plane direction in the image. The SEM image shows the fiber architecture with whole [0°-90°-0°]. Fibers between white dashed lines are horizontal, and other fibers are perpendicular to the image. Figure 2 shows a schematic of the architecture of the sample. The architecture is cross-ply [0°-90°-0°]s. ⊥ is a thickness direction, and 0° and 90° are in-plane directions.

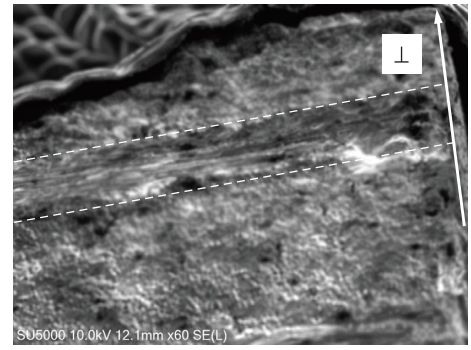

Figure 1: SEM image of the sample.

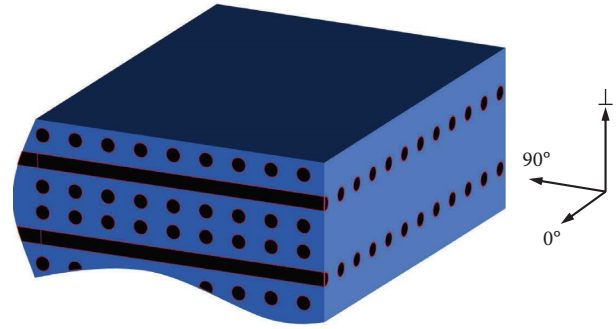

Figure 2: Schematic of the architecture of the sample.

2.2. Experimental Apparatus. The SiC_f/SiC composite has hard processing performance rates, but measuring the anisotropic thermal conductivity with normal measuring methods needs processing it to standard shape and size. To measure the thermal conductivity of the sample, a one-dimensional steady-state thermal conductivity measurement device was designed. In this study, all the testing works were conducted in the self-designed apparatus based on ASTM C201-93 [24]. The measurement was divided into the thermal conductivity in the out-of-plane direction (the thickness direction) and the in-plane direction. The heat flow loading direction was different along in-plane and thickness, so there were two heating chambers to be designed for the sample. The device measuring the thickness direction has already been calibrated by room temperature thermal conductivity using the flash method, and the device measuring the out-of-plane direction has been amended. As shown in Figure 3(a), the apparatus is used for measuring the thermal conductivity of the in-plane direction, and Figure 3(b) shows the heating chamber for measuring the out-of-plane direction. The apparatus mainly consists of a personal computer, an adjustable DC power supply, a converter, a water pump, a voltmeter, a temperature monitoring instrument, a circulating cooling water system, and two heating chambers. These chambers were composed of aluminum silicate fiber ceramic fiber insulation, which can effectively prevent the heat from diffusing into the outside air.

The schematic of chambers is shown in Figure 4(a), which was used for measuring the in-plane direction. Two samples were fixed in the chamber. The heating unit comprised a heat strip clamped between sample A and sample B, and the two sides of the sample were clamped using copper plates. The water-cooled plate was arranged on the other side of the copper plate, and the heat generated by the heat trip was taken away by circulating water. The current during the experiment was displayed by an adjustable DC power supply, and the voltage was measured in an electric heat strip with a voltmeter attached to the immediate end of the sample. The temperature distribution of the sample surface was measured by using 12 thermometers during heating. There were 4 thermometers on the upper surface of sample A and sample B and the lower surface of sample A. Thermometers were evenly arranged along the center line. Figure 4(b) shows the measurement of the out-of-plane direction. The sample was fixed in the chamber. Sample and heating unit aluminum of the same size was champed by using the guard board and copper board. There was a thermometer on the upper and lower surfaces and surface of the guard board. Each thermometer was in the center.

During sample assembly, all contact surfaces along heat flow were coated with thermal grease, eliminating contact gaps and reducing errors. The loading unit is adjusted until the results of the thermometer have no influence on the sample. During the measurement, the current and voltage of the DC power supply were adjusted to the output power, so the heating unit produced heat flow. The heat flows out of the sample from the heating unit to the cold plate.

During the measurement, the heat transfer rate was constant. The heat transfer rate was determined by the voltage and the current at the contact position between the heating part and the sample. The calculation formula of the heat flux q on the heating interface was

$$q = \frac{UI}{A}, \tag{1}$$

where q was heat flux, W/m^2; U was the voltage between heat strip, V; I was the current intensity, A; and A was the area of heating, m^2.

Figure 5 shows the arrangement of the thermometers measuring the temperature thermal conductivity of the in-plane. The position next to the heating unit was the starting

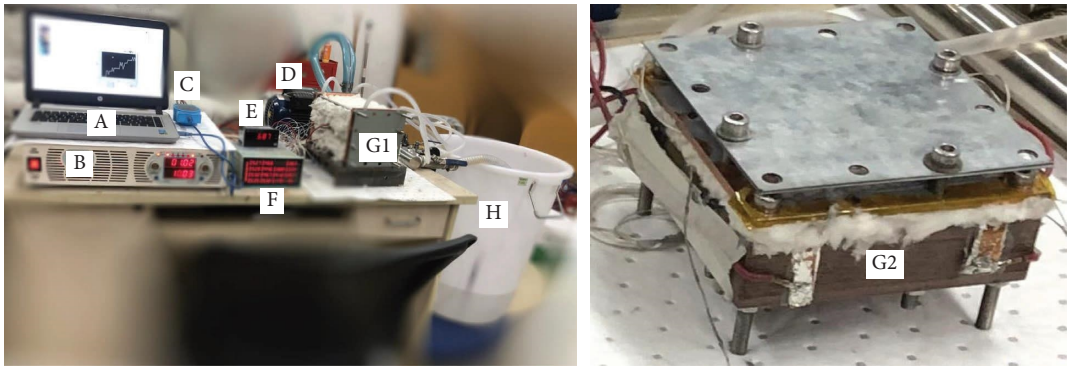

A-PC
B-DC power supply
C-Converter
D-Water pump
E-Voltmeter
F-Temperature monitoring instrument
G1-Heating chamber of out of plane direction
G2-Heating chamber of thickness direction
H-Water poll

(a) (b)

Figure 3: Thermal conductivity measurement apparatus.

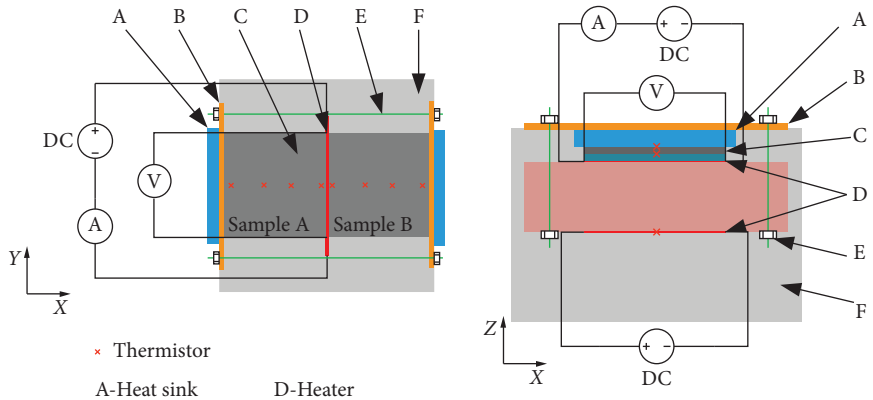

(a) (b)

Figure 4: Schematic of the chambers: (a) in-plane measurement; (b) out-of-plane measurement.

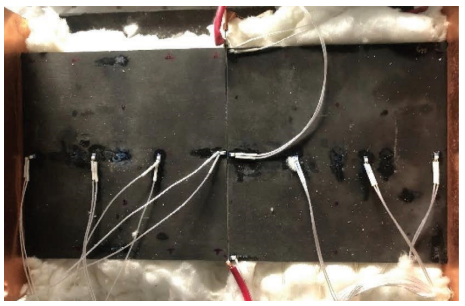

Figure 5: The PT100 probes on the sample in-plane direction.

point, the position next to the copper board was the endpoint, and four thermometers were arranged evenly along the center line of the sample surface. In addition, the four thermometers were also arranged on the lower surface of a sample. As shown in Figure 6, the aluminum plate was a heating unit, and the area of the aluminum plate is the same as the size of the sample. One side of the aluminum plate was pasted with a heating film, and a groove was present in the surface which was connected with the sample; the thermometer was in the groove. During the sample assembly process, the aluminum plate was filled with thermal grease to eliminate the influence of the gap on the measurement.

When measuring the thermal conductivity in the thickness direction, the electric heating film generates a stable heat transfer rate along the thickness direction. At the same time, it keeps the guard temperature equal to the temperature of the sample surface of the heating side. The heat transfer rate flows through the aluminum plate to generate a uniform heat flux. After the uniform heat flux flowed through the sample, a difference in temperature between the surface of the hot side and the cold side of the sample was generated. The heat was taken away from the water wall. The thermal conductivity in the measured thickness direction was calculated according to Fourier's law using the following equation:

$$\lambda_{\perp} = \frac{q\delta}{\Delta t}, \tag{2}$$

where $\lambda_{\perp}$ was the thermal conductivity of in-plane, $Wm^{-1}K^{-1}$; δ was the thickness of the sample, m; and Δt was the temperature difference, ˚C.

When measuring the thermal conductivity in the in-plane direction, the heating unit generated a stable heat transfer rate and uniform heat flux along the in-plane direction. The uniform heat flux equally flowed into sample A and sample B. A difference in temperature was generated along with the heat flux in samples. The heat is taken away through the water-cooled wall. After heating reached a steady state, a stable temperature field would be formed in the sample, at which time the temperature data were recorded. When heating reached a steady state, all the heat entering the sample was lost. Ideally, the whole heat flowed past samples along the direction of the heat flux, forming a uniform temperature gradient in the sample along the direction of the heat flux. In the actual measurement, the flat sample will have heat dissipation on the other four faces, so the surface temperature of the sample will decrease. The measurement temperature will be smaller than the idealistic temperature, and the resulting temperature gradient will make the experimental measurement of thermal conductivity larger. When heat dissipation is too large, the measured thermal conductivity result will have a large error, and surface heat dissipation cannot be ignored at this time. To correct the temperature experiment error caused by surface heat dissipation, the measured thermal conductivity was corrected. Considering that the sample was a square plate, the area of the heat dissipation surface in the direction of the

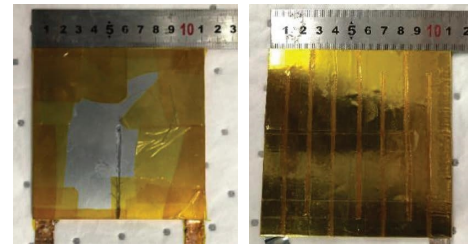

Figure 6: The heating plate of aluminum.

surface is much smaller than that of the heat dissipation faces in the thickness direction. To simplify the analysis, we only consider the heat dissipation from the heat dissipation faces in the thickness direction. If there is no heat dissipation on the surface of the sample, the temperature of the sample along the x position on the surface will be uniform. The temperature distribution along the x position can be expressed by the temperature at the center section of the thin plate, and the thermal conductivity of the sample along the direction of the surface can be calculated through the surface temperature distribution. If the surface had heat dissipation, the surface temperature at any x position would be lower than the medial temperature. The thermal conductivity of the sample should be calculated according to the medial temperature distribution of the center section of the sample. Heat dissipation at any location can be determined by the difference in temperature between the surface and the inside of the sample. To simplify the analysis, the following assumptions are made about the thermal conductivity of the plate when measuring the thermal conductivity within the sample surface:

(1) The heat loss density on the surface of the plate decreases linearly along the x-direction

(2) The temperature of the upper and lower faces in the thickness direction of the plate is equal

Based on the above hypotheses, the heat conduction of the plate in the in-plane direction can be regarded as one-dimensional steady-state heat conduction along the central section of the plate. Figure 7(a) shows a schematic diagram of the in-plane direction heat conduction of a single-sided thin plate. The temperature of the upper and lower faces of the plate is t_{sur}, and the temperature at the center of the plate is t_{mid}. The temperature distribution in the plate can be further simplified as one-dimensional heat conduction with heat dissipation. Figure 7(b) shows a schematic diagram of heat transfer in the plate. The heat dissipation on the upper and lower surfaces of the plate is added to one-dimensional heat conduction as an internal heat element. At any x position, the equation for heat conduction is written as follows:

$$\lambda \frac{\partial^2 t_{mid}}{\partial x^2} + \frac{\Phi_s}{\delta L dx} = 0, \tag{3}$$

where Φ_s is the total heat lost from the surface, W.

In the measurement, the water wall could be regarded as an isothermal wall, so the surface of the sample in contact with the water wall was also an isothermal wall. At $x = L$, it

could be known $t_{mid} = t_{sur}$, $\Phi_s = 0$. According to the assumption, $\Phi_s = 2\delta k(L - x)Ldx$ (k_1 is a constant, $k_1 \geq 0$). Then, the temperature distribution at the central section can be obtained:

$$t_{mid} = t_0 - \frac{UI}{2\lambda_x \delta L}x - \frac{k}{\delta\lambda_x}\left(Lx^2 - \frac{x^3}{3}\right), \quad (4)$$

where λ_x is the thermal conductivity of in-plane, $Wm^{-1}K^{-1}$; t_0 is the sample's temperature at the original in the middle section, °C.

Equation (5) can be obtained by transforming equation (4). At $x = 0$, equation (5) satisfies the one-dimensional Fourier law, which is the thermal conductivity when measuring temperature t_0. As x increases, the thermal conductivity calculation needs to subtract the second term on the left side of equation (5). Otherwise, the measured thermal conductivity will be too large. This formula shows that there is heat loss on the surface of the sample. With an increase of x, the difference in temperature at the central section of the sample will increase due to heat dissipation, so the correction value of the measured thermal conductivity will also increase. The thermal conductivity calculation does not need to subtract errors due to heat loss only at the beginning of heating. With the accumulation of heat loss along the heat flux direction on the surface, the difference in temperature between any two points along the heat flux direction will increase:

$$\lambda_x = -\frac{UI}{2\delta L}\frac{dx}{dt_{mid}} - \frac{2}{\delta}k\left(Lx - \frac{x^2}{2}\right)\frac{dx}{dt_{mid}}. \quad (5)$$

At any x position, it can be considered that the one-dimensional energy conservation equation could be satisfied in the Z direction. According to Assumption 2, the surface temperature at any X position and the medial temperature can satisfy the following equation:

$$t_{sur} = t_{mid} - \frac{k(L - x)}{4\lambda_\perp}\delta. \quad (6)$$

The surface temperature distribution at any x position can be described:

$$t_{sur} = t_0 - \frac{UI}{2\lambda_x \delta L}x - \frac{k}{\delta\lambda_x}\left(Lx^2 - \frac{x^3}{3}\right) - \frac{k(L - x)}{4\lambda_\perp}\delta. \quad (7)$$

According to the above analysis, the thermal conductivity at $x = 0$ was calculated by equation (7). The temperature at the $x = 0$ position was different when the heating power was different, and the result was the thermal conductivity of the sample at different temperatures. According to the temperature distribution, equation (7) is fitted with the experimental measurement temperature distribution. Finally, the thermal conductivity at t_0 was measured. The λ value, that is, the thermal conductivity of t_0, is measured by fitting to obtain different heating powers. During the measurement process, the sample temperature is considered to have reached a steady state when the temperature changes very little with time.

2.3. Thermal Conductivity Testing. Figure 8 shows the measurement of the sample surface temperature at different heating powers in the 0° and 90° directions and the fitting result of equation (7). The $x = 0$ position in the figure is the location of the heat strip. As x increases, the closer it is to the sink source, the lower the temperature. Due to the surrounding thermal insulation during the measurement, the heat flow in the sample can be seen as flowing out in the x direction from the position of the heating band to the water wall. According to Fourier's law of thermal conductivity, the temperature of the sample gradually decreases in the direction of heat flow. Since the thermal conductivity of the two samples is basically the same and the temperature at the sink source of the sample is the same water temperature, the heat flows evenly into the two samples and then flows out from the sink source. It can be seen from the measurement results that the temperature is basically the same at the same x position of the sample. Heat loss along the thickness of the sample accumulates along x during the experiment, while the heat loss at the $x = 0$ position is zero. Therefore, the thermal conductivity at the $x = 0$ position is the accurate thermal conductivity of the sample, and the thermal conductivity of the sample at the corresponding temperature can be obtained by fitting the measurement result with equation (7).

Figure 9 shows the thermal conductivity of the sample decreases with an increase in temperature. Because the thermal conductivity of the SiC matrix decreases with temperature, while the thermal conductivity of SiC fiber increases with temperature, the overall impact on the thermal conductivity of the sample is smaller than that of the SiC matrix. Due to the difference in thermal conductivity of the SiC matrix, fiber, and interface layer, the thermal conductivity of the sample is different in the thickness direction and the 0° and 90° directions in the plane. The thermal conductivity of the material in the thickness, in-plane 0°, and in-plane 90° directions at room temperature is 24.9 $W^{-1}K^{-1}$, 28.5 $W^{-1}K^{-1}$, and 31.1 $W^{-1}K^{-1}$, respectively.

3. Finite Element Analysis

Numerical models have been widely applied to predict the properties of composites at hierarchical levels. In this paper, numerical models based on RVE were built at the microscale. Figure 10 shows the numerical models of the SiC_f/SiC composites in different scales. The sample was raised using [0-90-0]s configurations, and [0-90-0] was crossed with 3 unidirectional [0°]s. Therefore, the thermal properties of the entire component model were sampled as [0-90-0] ply. Its thermal conductivity could be calculated unidirectionally. The unidirectional thermal conductivity was calculated as the material parameters of the microscale model. The microscale model consisted of SiC fibers, the silicon matrix, and the BN interface layer.

In this study, the RVE model was the hexagonal unit cell, which consisted of four-quarter circles and rings. The geometric parameters of the hexagonal unit cell were as follows: l_1 and l_2 were the edge lengths of the hexagonal unit cell. The fiber diameter d of the microscale RVE model was

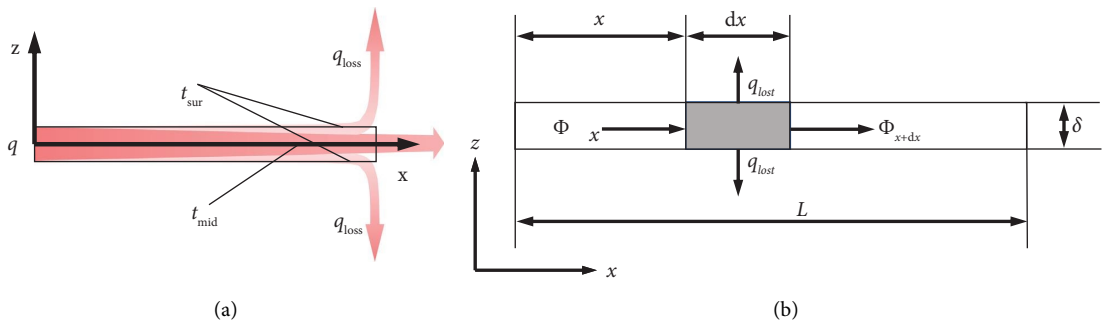

Figure 7: The schematic of thermal conduction of sample in the in-plane direction.

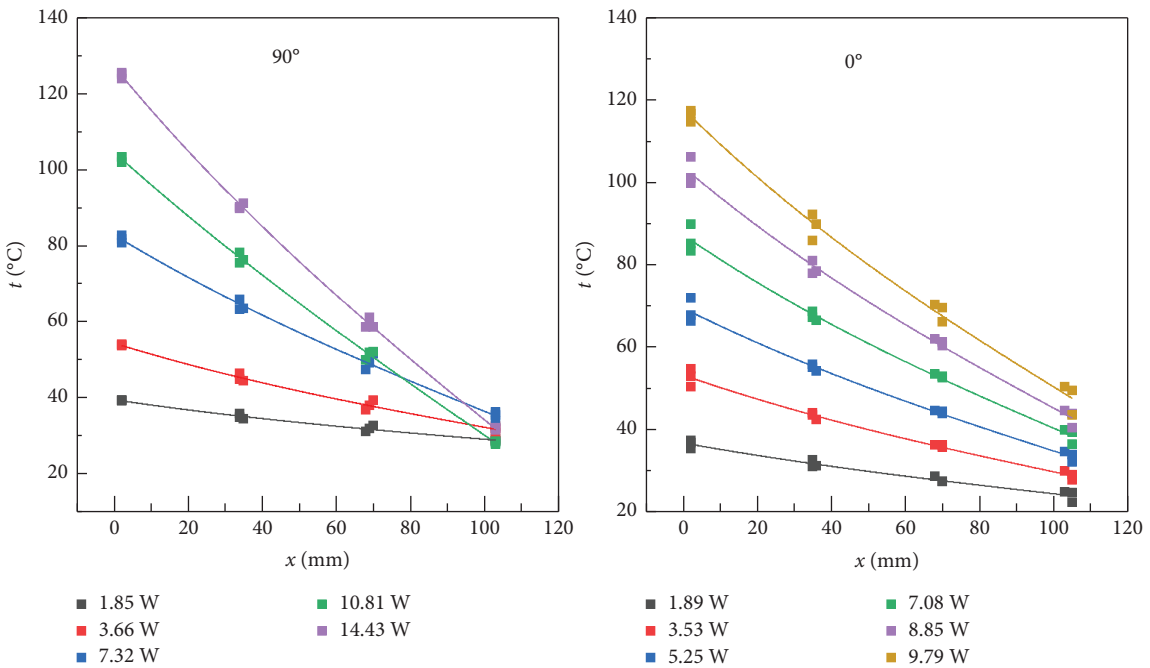

Figure 8: Experimental temperature results on the surface of in-plane.

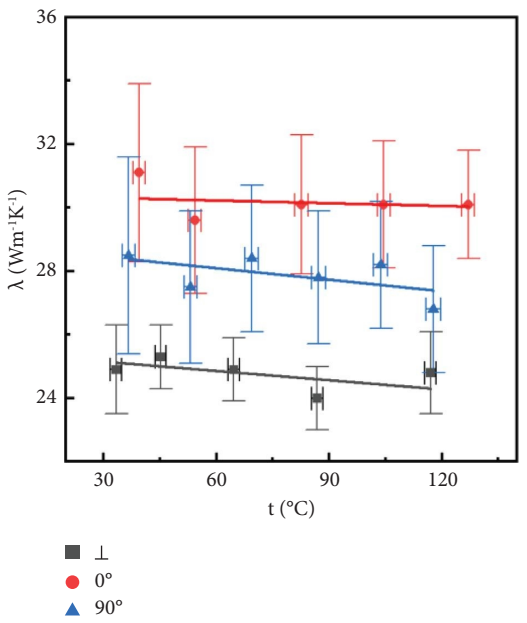

Figure 9: The experiment result of thermal conductivity.

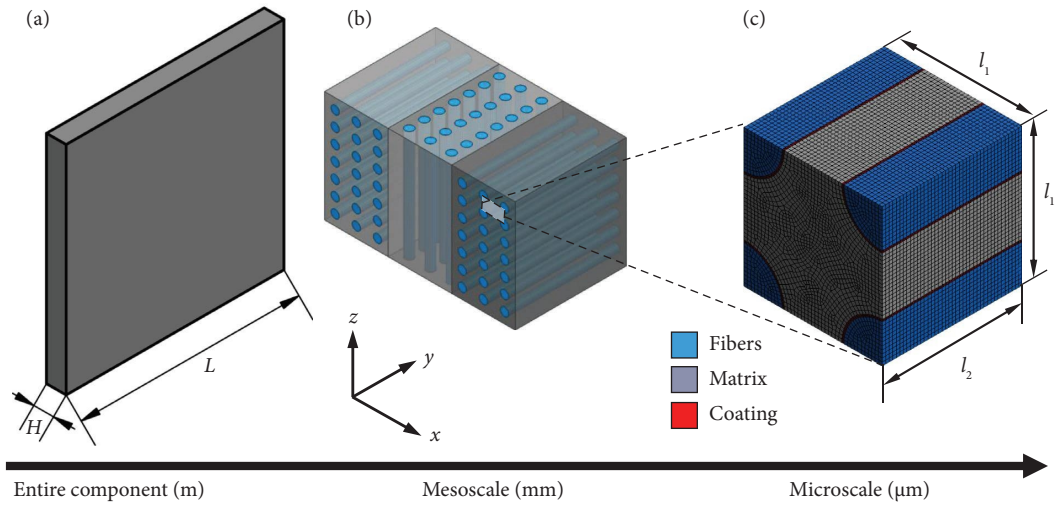

Figure 10: Schematic diagram of the sample: (a) sample; (b) 0°-90°-0° ply; (c) RVE model of subplyer.

defined. After checking for convergence, the numbers of nodes and elements were found to be 487065 and 101520:

$$V_f = \frac{\pi d^2}{4l_2^2}. \tag{8}$$

As shown in Table 1, the side lengths of the RVE model were l_1 and l_2, the fiber diameter was d, the volume fraction of the fiber in the sample was V_f, and the thickness of the interface layer between the fiber and the matrix was δ. Table 1 shows the relevant dimensions of the RVE model.

During the sample fabrication, the SiC matrix contains voids and impurities such as Si, so the thermal conductivity of the SiC matrix was uncertain. In this research, the thermal conductivity of the SiC matrix was predicted, and the result is shown in Table 2. As shown in Figure 11, the SiC fibers were distributed in the SiC matrix randomly. Choosing an area along the out-of-plane direction builds a numerical model, and then, we predicted the thermal conductivity of the SiC matrix according to the thermal conductivity of out-of-plane directions by experiment. Figure 12 shows the temperature distribution, and its temperature gradient is nonuniform because the thermal conductivity of SiC fibers and the BN interface layer is less than that of the SiC matrix.

The thermal conductivity of the SiC fiber, BN interface layer, and SiC matrix can be regarded as isotropic, and its parameters are shown in Table 2.

The calculation ignores the thermal resistance of contact between different materials in the RVE model and only considers the influence of the thermal conductivity on the temperature field of the RVE model. The temperature distribution of the RVE model was calculated using FEA, the temperature distribution of the elements in the grid was calculated according to equation (9), and the heat flow density was calculated according to equation (10). According to the geometric characteristics of the RVE model, the thermal conductivity of the RVE model in the x, y, and z directions was calculated, respectively. When calculating,

Table 1: Specifications of the RVE model in the SiC_f/SiC composite sample.

Fibers (μm)		Thickness of the interface layer (μm)	Unit cell (μm)	
d	V_f	δ	l_1	l_2
10.9	24.0%	0.3	19.7	20.0

Table 2: Thermal conductivity of the sample's constituents.

	SiC fibers [25]	BN interface layer [26]	SiC matrix
TC ($Wm^{-1}K^{-1}$)	$t = 27°C$, 4.75 $t = 100°C$, 5.66 $t = 200°C$, 6.13	0.58	$t = 27°C$, 42.7 $t = 127°C$, 40.6

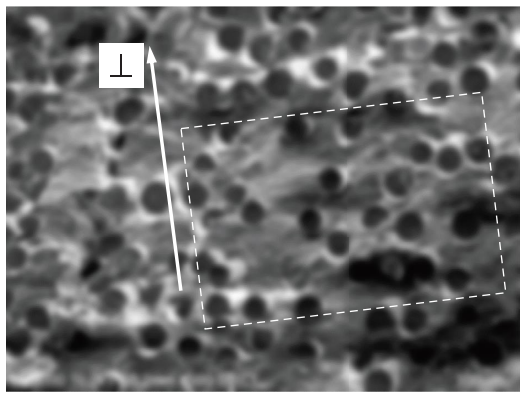

Figure 11: Image of fiber distribution.

the wall conditions on both sides of the same direction were uniform wall temperature, the temperature difference between the two sides was 1°C, and the heat flow through the wall surface was obtained after calculation; the thermal conductivity of the RVE model in different directions was calculated by the result (2):

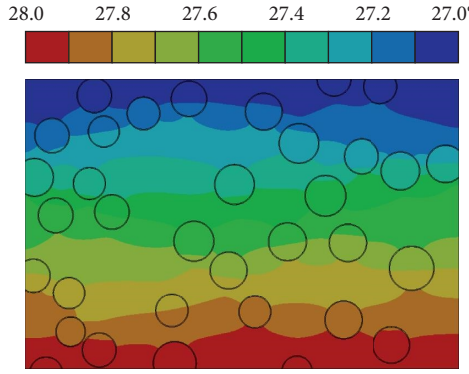

Figure 12: The temperature of the SiC_f/SiC composite.

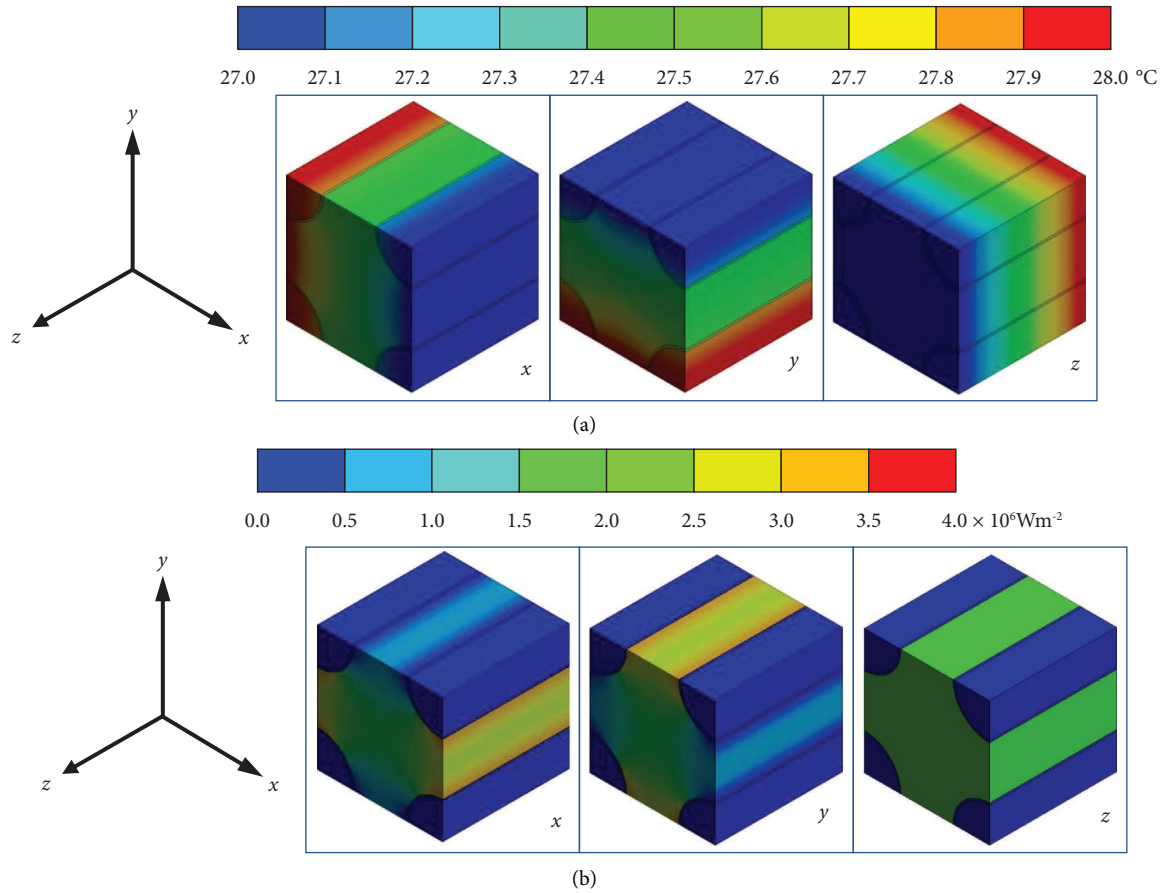

Figure 13: Result of numerous (a) temperature distributions and surface heat flux distributions in the axis direction and (b) temperature distributions and surface heat flux distributions in the radius direction.

$$\frac{\partial}{\partial x}\left(\lambda_x \frac{\partial t}{\partial x}\right) + \frac{\partial}{\partial y}\left(\lambda_y \frac{\partial t}{\partial y}\right) + \frac{\partial}{\partial z}\left(\lambda_z \frac{\partial t}{\partial z}\right) = 0, \quad (9)$$

where λ_x, λ_y, and λ_z was conductivity in the elements x, y, and z directions,

$$\{q\} = -[\lambda]\{a\}, \quad (10)$$

where $\{q\}$ was the heat flux vector in x, y, and z directions, $\{\lambda\}$ was the thermal conductivity matrix in x, y, and z directions, and $\{a\}$ was the thermal gradient vector in x, y, and z directions.

The steady-state transfer simulations were carried out to predict the thermal conductivity at the silicon certificate fiber tow level (microscale). The temperature contour and the heat flux distribution in the x, y, and z directions at room temperature are illustrated in Figure 13.

The temperature distribution of the RVE model when the heat conducts along the x, y, and z directions is shown in Figure 13(a). For conduction delay along the z direction, the model shows a more uniform temperature distribution in Figure 13(b). When the heat is conducted along the x, y, and z directions, the heat flux distribution of the RVE model

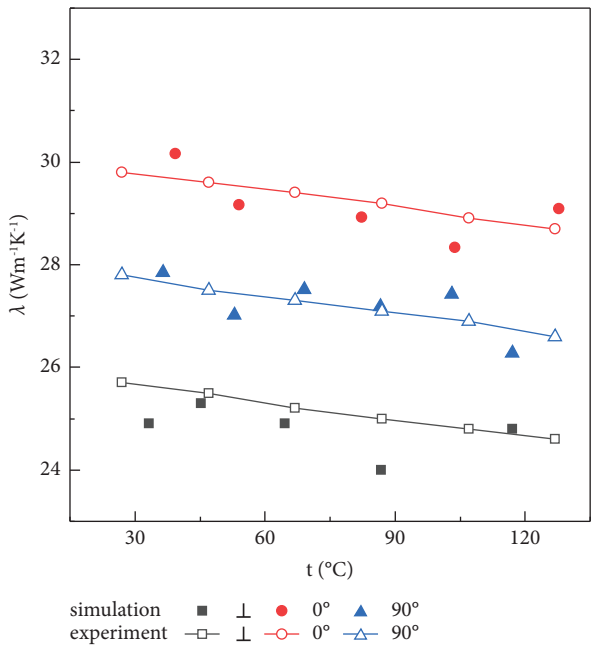

Figure 14: Thermal conductive behaviors of a sample.

Table 3: Results of thermal conductivity.

	0°	90°	⊥
Experience ($Wm^{-1}K^{-1}$)	27.9	30.2	24.8
Simulation ($Wm^{-1}K^{-1}$)	27.2	29.3	25.1
Deviation (%)	−2.5	−3.0	1.2

along the corresponding directions. When the heat is conducted along the x and y directions, the heat flow is mainly concentrated in the matrix at the beginning, and the heat flux first decreases and then increases. When conducted along the z direction, the heat flow is evenly distributed in the matrix. It can be seen from the calculation results that, in the process of heat conduction, the temperature distribution in the fiber was more uniform than that in the matrix and that heat flow was mainly derived from the matrix. The heat flow density was concentrated between the fibers when the heat flow passes through the fiber, and a large temperature difference will occur at this time.

Since the diameter of SiC ceramic fibers was much smaller than that of single-layer CMCs, and ceramic fibers can be considered to be uniformly distributed, the thermal conductivity of single-layer CMCs was simplified as a thermal conductivity anisotropic flat plate. The formula was

$$\begin{cases} \lambda_0 = \dfrac{\left(\lambda_y + 2\lambda_z\right)}{3}, \\ \lambda_{90} = \dfrac{\left(2\lambda_y + \lambda_z\right)}{3}, \\ \lambda_\perp = \lambda_x. \end{cases} \tag{11}$$

Figure 14 shows the thermal conductivity of the numerical calculation using equation (11) and experiment results. For the thermal conductivity of a single-layer sample, axial thermal conductivity was greater than radial thermal conductivity. The experimental measurement sample was laid by a single-layer material through 0°-90°-0°, which causes the axial distribution and radial distribution of the sample in different directions to be different, so the thermal conductivity in different directions was different. Thermal conductivity along fiber direction was great than the other direction. Therefore, the thermal conductivity in 0° direction was the largest and in the out of plane direction was the smallest.

Table 3 shows the average value of the experimental measurement results and the numerical simulation. It can be seen from the results that the relative error between the experimental measurement results and the numerical simulation results was less than 3%. In the process of sample manufacturing, the fiber distribution cannot be guaranteed to be uniform, and the RVE model deviates from the actual sample, so the experimental result is the error of the numerical simulation result.

4. Conclusion

In this work, the thermal conductivity of in-plane and out-of-plane directions of [0-90-0]s SiC_f/SiC flat plates was measured by the steady-state measurement method. In addition, we proposed an improved FEA method to study the thermal behavior of laminated SiC_f/SiC composites. SiC matrix conductivity was predicted according to the thermal conductivity in the thickness direction by FEA; then, the thermal conductivity in the in-plane direction was predicted by the FEA method. The main conclusions obtained in this paper are as follows: (1) the thermal conductivity along the fiber radial direction was greater than it was in the axial direction. The thermal conductivity of the SiC matrix had a significant effect on the macroscopic thermal conductivity of the composite material. (2) The thermal conductivity decreases with an increase in temperature. The thermal conductivity of the SiC_f/SiC composites of the in-plane direction at room temperature was 31.1 $Wm^{-1}K^{-1}$ and 28.5 $Wm^{-1}K^{-1}$, and the thermal conductivity in the thickness direction was 24.9 $Wm^{-1}K^{-1}$. (3) The improved FEA method was employed to effectively predict the thermal conductivity of the SiC matrix and the SiC_f/SiC composite. The results of the experiment showed a good agreement with improved FEA.

In future work, the thermal conductivity of higher temperatures of the sample will be carried out by the improved FEA method.

Data Availability

Data are available within the article.

Conflicts of Interest

The authors declare that they have no conflicts of interest.

References

[1] X. Wang, X. Gao, Z. Zhang, L. Cheng, H. Ma, and W. Yang, "Advances in modifications and high-temperature applications of silicon carbide ceramic matrix composites in aerospace: a focused review," *Journal of the European Ceramic Society*, vol. 41, no. 9, pp. 4671–4688, 2021.

[2] O. Gavalda Diaz, G. Garcia Luna, Z. Liao, and D. Axinte, "The new challenges of machining ceramic matrix composites (cmcs): review of surface integrity," *International Journal of Machine Tools and Manufacture*, vol. 139, pp. 24–36, 2019.

[3] M. S. B. Hoque, Y. R. Koh, K. Aryana et al., "Thermal conductivity measurements of sub-surface buried substrates by steady-state thermoreflectance," *Review of Scientific Instruments*, vol. 92, no. 6, Article ID 064906, 2021.

[4] A. N. Karim, P. Johansson, and A. Sasic Kalagasidis, "Determination of the Anisotropic thermal Conductivity of an Aerogel-Based Plaster Using Transient Plane Source Method," *Journal of Physics: Conference Series*, vol. 2069, 2021.

[5] A. A. Trofimov, J. Atchley, S. S. Shrestha, A. O. Desjarlais, and H. Wang, "Evaluation of measuring thermal conductivity of isotropic and anisotropic thermally insulating materials by transient plane source (hot disk) technique," *Journal of Porous Materials*, vol. 27, no. 6, pp. 1791–1800, 2020.

[6] Y. Jannot, A. Degiovanni, V. Schick, and J. Meulemans, "Apparent thermal conductivity measurement of anisotropic insulating materials at high temperature by the parallel hot-wire method," *International Journal of Thermal Sciences*, vol. 160, Article ID 106672, 2021.

[7] A. Elkholy and R. Kempers, "An accurate steady-state approach for characterizing the thermal conductivity of additively manufactured polymer composites," *Case Studies in Thermal Engineering*, vol. 31, Article ID 101829, 2022.

[8] A. Elkholy, M. Rouby, and R. Kempers, "Characterization of the anisotropic thermal conductivity of additively manufactured components by fused filament fabrication," *Progress in Additive Manufacturing*, vol. 4, pp. 497–515, 2019.

[9] K. E. de Conde, A. C. do Prado, E. C. Garcia, and E. dos Santos Magalhães, "Experimental assessment of laminated material anisotropic thermal conductivity," *International Communications in Heat and Mass Transfer*, vol. 128, Article ID 105593, 2021.

[10] H. Zhang, K. Wu, G. Xiao, Y. Du, and G. Tang, "Experimental study of the anisotropic thermal conductivity of 2d carbon-fiber/epoxy woven composites," *Composite Structures*, vol. 267, Article ID 113870, 2021.

[11] R. Penide-Fernandez and F. Sansoz, "Anisotropic thermal conductivity under compression in two-dimensional woven ceramic fibers for flexible thermal protection systems," *International Journal of Heat and Mass Transfer*, vol. 145, Article ID 118721, 2019.

[12] K. L. Kai Dong, Q. Zhang, and B. Gu, "Experimental and numerical analyses on the thermal conductive behaviors of carbon fiber/epoxy plain woven composites," *International Journal of Heat and Mass Transfer*, vol. 209, 2016.

[13] M. Iasiello, N. Bianco, W. K. S. Chiu, and V. Naso, "Thermal conduction in open-cell metal foams: anisotropy and representative volume element," *International Journal of Thermal Sciences*, vol. 137, pp. 399–409, 2019.

[14] X. Zhao, F. Guo, B. Li, G. Wang, and J. Ye, "Multiscale simulation on the thermal response of woven composites with hollow reinforcements," *Nanomaterials*, vol. 12, no. 8, p. 1276, 2022.

[15] Z. Sun, Z. Shan, T. Shao, and Q. Zhang, "Numerical analysis of out-of-plane thermal conductivity of c/c composites by flexible oriented 3d weaving process considering voids and fiber volume fractions," *Journal of Materials Research*, vol. 35, no. 14, pp. 1888–1897, 2020.

[16] M. Ahmadi, R. Ansari, and M. K. Hassanzadeh-Aghdam, "Finite element analysis of thermal conductivities of unidirectional multiphase composites," *Composite Interfaces*, vol. 26, no. 12, pp. 1035–1055, 2019.

[17] J. Binner, M. Porter, B. Baker et al., "Selection, processing, properties and applications of ultra-high temperature ceramic matrix composites, uhtcmcs - a review," *International Materials Reviews*, vol. 65, no. 7, pp. 389–444, 2020.

[18] T.-Y. Cho and Y.-W. Kim, "Effect of grain growth on the thermal conductivity of liquid-phase sintered silicon carbide ceramics," *Journal of the European Ceramic Society*, vol. 37, no. 11, pp. 3475–3481, 2017.

[19] W. Li, C. Cui, J. Bao, G. Zhang, S. Li, and G. Wang, "Properties regulation of sic ceramics prepared via stereolithography combined with reactive melt infiltration techniques," *Ceramics International*, vol. 47, no. 24, pp. 33997–34004, 2021.

[20] J. Wang, Y. S. Chen, Y. J. Feng et al., "Influence of porosity on anisotropic thermal conductivity of sic fiber reinforced sic matrix composite: a microscopic modeling study," *Ceramics International*, vol. 46, no. 18, pp. 28693–28700, 2020.

[21] E. K. Pek, J. Brethauer, and D. G. Cahill, "High spatial resolution thermal conductivity mapping of sic/sic composites," *Journal of Nuclear Materials*, vol. 542, Article ID 152519, 2020.

[22] K. Hye-gyu and J. Wooseok, "Thermal conductivity of a thick 3d textile composite using an rve model with specialized thermal periodic boundary conditions," *Functional Composites and Structures*, vol. 3, no. 16, Article ID 015002, 2021.

[23] H. Wu, M. Chen, X. Wei, M. Ge, and W. Zhang, "Deposition of bn interphase coatings from b-trichloroborazine and its effects on the mechanical properties of sic/sic composites," *Applied Surface Science*, vol. 257, no. 4, pp. 1276–1281, 2010.

[24] ASTM C201 – 93, *Standard test method for thermal conductivity of refractories*, ASTM, West Conshohocken, PY, USA, 2019.

[25] G. E. Youngblood, R. H. Jones, and W. Kowbel, "Optimizing the Transverse thermal Conductivity of 2d-Sicf/sic Composites II. Experimental," *Journal of Nuclear Materials*, vol. 307, 2002.

[26] H. Wang, S. Gao, S. Peng et al., "Kd-s sicf/sic composites with bn interface fabricated by polymer infiltration and pyrolysis process," *Journal of Advanced Ceramics*, vol. 7, no. 2, pp. 169–177, 2018.